Available online at www.sciencedirect.com
ScienceDirect
International Journal of Thermal Sciences 46 (2007) 1142–1152
International Journal of Thermal Sciences
www.elsevier.com/locate/ijts

Sensing and modeling techniques for microscale transport

Sung Jin Kim *, Dong-Kwon Kim

Department of Mechanical Engineering, Korea Advanced Institute of Science and Technology, Taejon, 305-701, South Korea

Received 16 June 2006; received in revised form 9 January 2007; accepted 9 January 2007

Available online 12 April 2007

Abstract

In the present study, three types of micro-sensors developed for experimental investigation of fluid flow and heat transfer in microstructures are introduced. The micro-sensors can be used to measure temperature distributions at the surface of a microstructure and mass flow rates passing through it. It is followed by a description of a method for modeling transport phenomena in microstructures. The modeling technique, based on the averaging method, is illustrated in thermal design and optimization of a microstructure.

Keywords: Micro-sensors; Averaging method; Microscale transport

1. Introduction

The transport and interactions of matter in a microstructure always involve flow and/or exchange of energy because some energy in the form of heat is generated through any irreversible transport phenomena, as suggested by the second law of thermodynamics [1]. There are many micro-mechanical systems for which thermal aspects are even more critical. These include microstructures encountered in biological reactions and processes, fuel cells, high-performance heat exchangers and cooling devices, chemical processes and so on [2–4]. Therefore, many investigators have experimentally and numerically studied fluid-flow and heat-transfer characteristics of microsystems. In their experimental and numerical investigations, they have suggested various experimental techniques and numerical models. However, there still exist a lot of limitations in their experimental tools and simulation methods. For example, it is not easy to measure the temperature of a microstructure and the mass flow rate of a fluid passing through it due to its small size. This difficulty has caused confusion with some investigators who claimed that transport phenomena cannot be predicted by conventional theories based on continuum mechanics. In addition, modeling can be cumbersome because of the complex topology of microstructures. Complicated models for analyzing fluid-flow and heat-transfer characteristics of a microstructure require tedious effort and a lot of computational time. Therefore, it is necessary to develop a simple but accurate modeling method for analyzing thermal characteristics of microstructures encountered in micro-mechanical engineering.

In this paper, sensing and modeling techniques developed for investigating transport phenomena in microstructures are introduced. For this purpose, the present paper consists of two parts. The first part covers three types of microscale sensors developed for experimental investigations. These micro-sensors, which are applicable to measuring temperature distributions at the surface of a microstructure and the mass flow rate of a fluid passing through it, are described. Specifically, the micro-thermal sensor array, diode temperature sensor array, and microscale mass flow sensor are presented. The characteristics and manufacturing processes for these micro-sensors are explained. In the second part, a microchannel heat sink is chosen as a case study to illustrate the method in the thermal design and optimization of a microstructure. A modeling technique based on the averaging method is described, which can be conveniently used to analyze fluid flow and heat transfer in a microstructure.

2. Sensors for experimental investigations

2.1. Micro-thermal sensor array

When it is necessary to measure the surface temperature of micro-mechanical systems, temperature sensors based on elec-

* Corresponding author. Tel.: +82 42 869 3043; fax: +82 42 869 8207.
E-mail address: sungjinkim@kaist.ac.kr (S.J. Kim).

1290-0729/$ – see front matter
doi:10.1016/j.ijthermalsci.2007.01.024

Nomenclature

a	wetted area per volume	m^{-1}
c_f	heat capacity of fluid	kJ/kg K
Da	Darcy number $\equiv K/H^2$	
D_h	hydraulic diameter	m
h	heat transfer coefficient based on the bulk-mean temperature	W/m^2 K
h_i	interstitial heat transfer coefficient	W/m^2 K
H	channel height	m
k	conductivity	W/m K
K	permeability	m^2
L	length of microchannel	m
m	mass flow rate	kg/s
Nu	Nusselt number for the fully-developed flow	
p	pressure	Pa
P	dimensionless pressure $\equiv (K/\varepsilon\mu_f u_m)d\langle p\rangle^f/dx$	
P_p	pumping power	W
q	heat transfer rate	W
q_w	heat flux over the bottom surface	W/m^2
R_θ	thermal resistance	K/W
T_b	temperature of microchannel base	K
T_f	bulk-mean temperature of fluid	K
T_w	wall temperature	K
u	velocity	m/s
u_m	mean velocity in the fluid region	m/s
U	dimensionless velocity $\equiv \langle u\rangle^f/u_m$	
w_c	channel width	m
w_w	fin thickness	m
W	width of microchannel	m
x, y, z	Cartesian coordinate system	
Y	dimensionless vertical coordinate, y/H	
$\langle\rangle^f$	volume-averaged value over the fluid region	
$\langle\rangle^s$	volume-averaged value over the solid region	

Greek symbols

ε	porosity	
μ	viscosity	kg/m s
θ	dimensionless temperature	
$\theta_{f,b}$	dimensionless bulk mean temperature of fluid	
ρ	density	kg/m^3

Subscripts

cap	capacity
conv	convective
e	effective conductivity
f	fluid
i	interstitial
s	solid
tot	total
∞	value for the flow between parallel plates subject to a constant heat flux

trical, optical and radiation characteristics of the sensor have been typically employed [2]. For example, many investigators [3–5] have used commercial thermocouples with various bead sizes for measuring the surface temperature of microstructures because of their convenience. However, commercial thermocouples, which have a thickness of several hundred microns, are not appropriate because it is impossible to attach a thermocouple to an exact location at the surface without modifying the surface geometry, let alone measure the surface temperatures at many locations. Hence to use commercial thermocouples for measuring the surface temperatures of a microstructure is not practical. In order to compensate for these disadvantages, many investigators have developed various thermal sensors such as micro-RTD (resistance temperature detector) sensors and diode sensors [6–9].

Yeh [6] used micro-RTD sensors based on platinum. The fabrication of this type of micro-RTD sensors starts with the thermal growth of an oxide dielectric layer upon which a PR (photoresist) mask is then used to pattern sensors, and then platinum is deposited by a sputtering process. The sensors are finally manufactured by using a chemical lift-off process. However, sensor leads of the micro-RTD sensors should not be made of platinum but of other materials, whose electrical resistance is nearly constant regardless of the temperature variation. This is due to the fact that the electrical resistance of a sensor cannot be exactly measured if the electrical resistances of both a sensor and sensor leads depend on the temperature variation. In addition, these sensors require difficult calibration processes.

In this paper, a micro-thermal sensor array manufactured through simple and convenient microfabrication processes is introduced for measuring temperature distributions at the base of microscale structures. The micro-thermal sensor array has 25 temperature sensors in an area of 5 mm × 5 mm on a silicon wafer. The operating principle for temperature measurement with the micro-thermal sensor array is the well-known Seebeck effect. The Seebeck effect refers to the generation of a voltage potential, or emf (electromotive force) in an open circuit consisting of two dissimilar materials due to a temperature difference between junctions, which are the contacting points of the two materials [10].

The micro-thermal sensor array uses two materials, alumel and chromel, to cause the Seebeck effect. Fig. 1 illustrates microfabrication processes for depositing alumel and chromel on a silicon wafer. The processes start with the thermal growth of a silicon dioxide film that acts as an electrical insulating layer and has a thickness of 200 nm (step (a)). In steps (b) and (d) of Fig. 1, two stainless steel masks with different patterns, instead of sophisticated PR masks, are used to deposit alumel and chromel on a silicon wafer. After a couple of sputtering processes and a mechanical lift-off process are sequentially conducted, the alumel and chromel lines with a thickness of 5000 Å are complete. A photograph of the micro-thermal sensor array is shown in Fig. 2. The size of a junction of the micro-

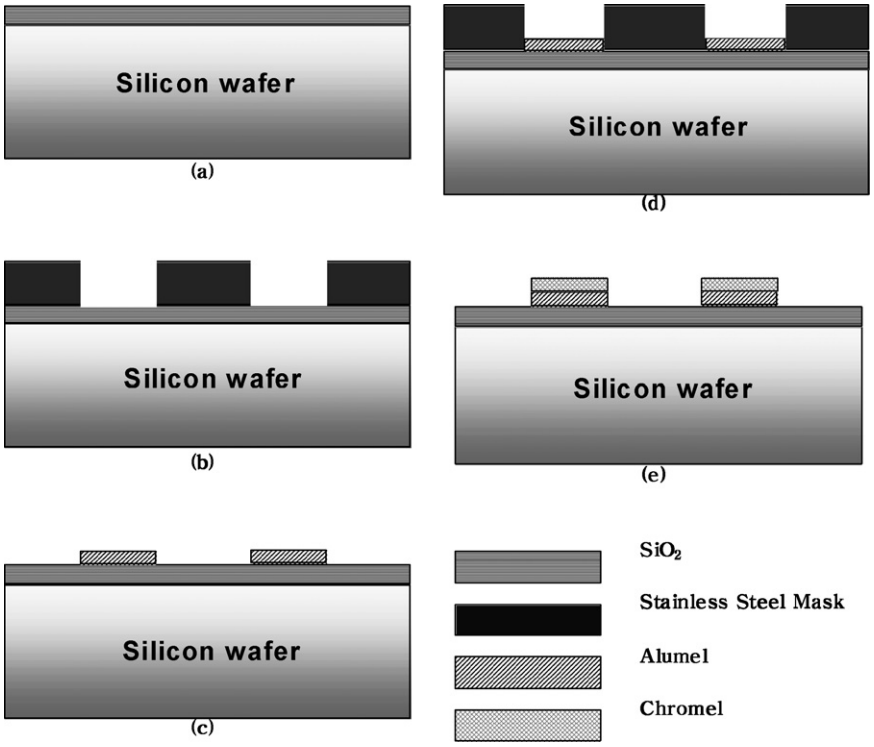

Fig. 1. Microfabrication processes for the micro-thermal sensor array.

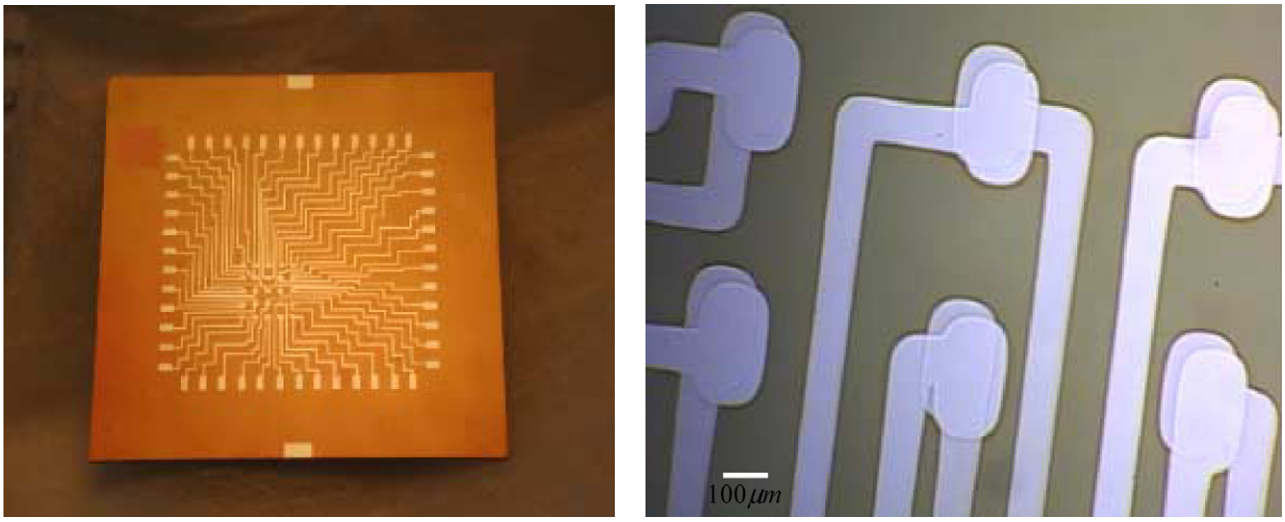

(a) (b)

Fig. 2. Micro-thermal sensor array. (a) Microfabricated micro-thermal sensor array. (b) Junction of micro-thermal sensor array.

thermal sensor array is 170 μm × 300 μm, as shown in the inset of Fig. 2. The surface temperature can be measured at 25 junctions by using the Seebeck effect, as mentioned previously. Fig. 3 shows a temperature distribution measured experimentally over a quarter area of the base of the microchannel heat sink subject to an impinging jet [11].

The micro-thermal sensor array has two advantages compared with other sensors previously mentioned. The first advantage is that the manufacturing processes are very simple and convenient. The second advantage is that calibration of the micro-thermal sensor array is not necessary if the accuracy of the micro-thermal sensor array is to be the same as that of a standard thermocouple. This is because the micro-thermal sensor array has the same characteristics as a K-type thermocouple. The size of the thermocouple junction in this array can be reduced further if the microfabrication processes similar to what have been used in Shi et al. [12] are adopted.

2.2. Diode temperature sensor array

In the previous section, the advantages of the microthermal sensor array that has been developed to measure the temper-

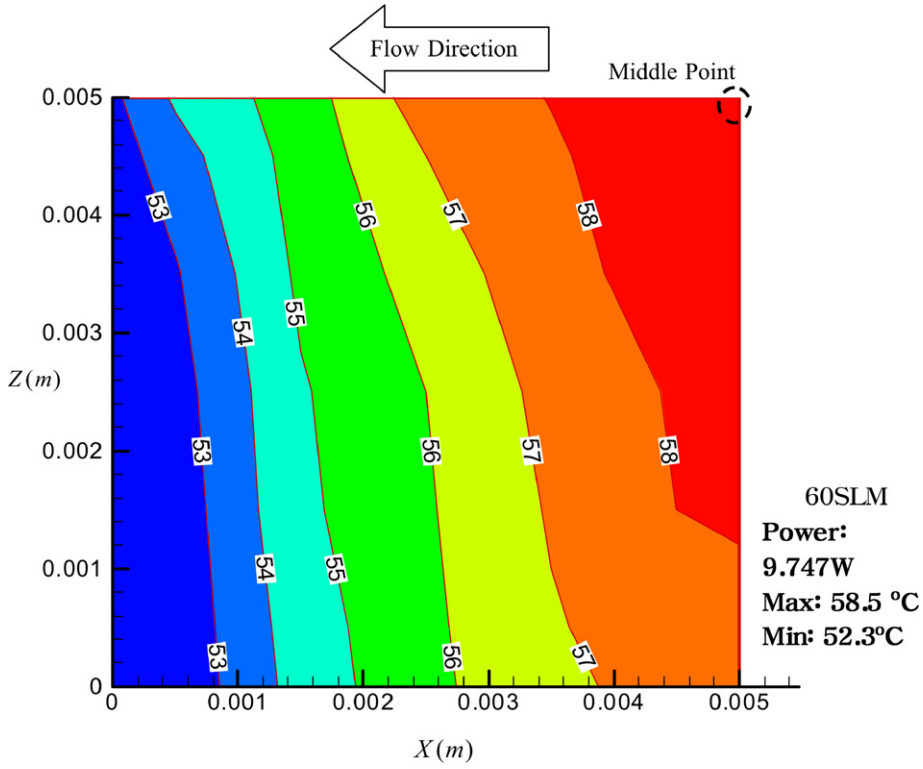

Fig. 3. Temperature distribution measured on the base of the microchannel heat sink subject to an impinging jet.

ature distribution of a microstructure are described. However, the microthermal sensor array is not free from limitations: each thermocouple junction needs two lead wires and two interconnection pads. This means that 2000 lead wires and 2000 interconnection pads are required if we want to measure temperatures at 1000 locations in a small area, which in turn causes a lot of trouble, enough to make a micro-thermocouple sensor array or a micro-RTD sensor array impractical.

To overcome this demerit of micro-thermocouple sensor arrays, a DTSA (diode temperature sensor array) has been developed. Use of silicon diodes to measure temperature is nothing new. They have been used to measure temperatures in electronics cooling and cryogenics applications. Silicon diodes typically have a forward voltage drop of 0.7 V that decreases by 2 mV for every 1 °C increase in temperature near room temperature. The voltage drop across a diode is approximately proportional to the inverse of the absolute temperature of the diode for a wider range of temperatures [13]. It is possible with the DTSA to detect temperatures at many more points in a given area than with the micro-thermocouple array, because the voltage drop across the diodes in the array can be obtained by scanning across the array. This is similar to the scanning (or decoding) technique frequently used for a DRAM memory cell array. The scanning technique enables DTSA to measure temperatures at 1024 points with only 64 interconnection pads instead of 2048 interconnection pads that would be used for the RTD or thermocouple sensor array.

Many investigators [7–9] have developed diode sensors. In particular, Kim et al. [9] developed a diode sensor array in order to study boiling heat transfer phenomena. The diode sensor array that they developed has 32 × 32 array points in an area of 3.2 mm × 3.2 mm, and the size of each diode is 100 μm × 100 μm. They were not able to drive all of the 32 × 32 array points. Only 16 diodes are properly operated due to manufacturing problems. The DTSA that we have developed is an extension of their work. The DTSA has 32 × 32 array points in an 8.0 mm × 8.0 mm area, as shown in Fig. 4. The size of each diode in the DTSA is 50 μm × 50 μm, as shown in the inset of Fig. 4. Square-shaped objects and wide lines in this figure denote diodes and heaters, respectively. Eight heaters made of poly-silicon are added onto a silicon wafer and controlled individually to maintain a uniform temperature distribution across the DTSA. The resistance of the heaters is designed to be 1 KΩ. In order to package the DTSA in a BGA (ball grid array) package or a stud bump flip chip package, the pad size is designed to be 600 μm × 600 μm, and 80 interconnection pads are shown in Fig. 4. The DTSA and the heaters are electrically connected to the driving circuitry through the 80 pads: 64 pads for the diodes and 16 for the heaters.

The circuitry for scanning the diodes and conditioning the signals from them in the DTSA consists of a DSP controller, two FPGAs, an amplifier, a power driver, and analog MUXs (multiplexers), as shown in Fig. 5. The FPGA1 is used for selecting which one of the 32 × 32 diodes is going to be measured. The measured voltage drops across the diodes are multiplexed into one signal through the analog MUX. This signal is amplified in the amplifier. The DSP controller is used for A/D conversion of the voltage drop (or temperature) signals and sends a control signal to the FPGA2. Then the FPGA2 generates PWM (pulse-width modulation) signals and sends them to the heaters

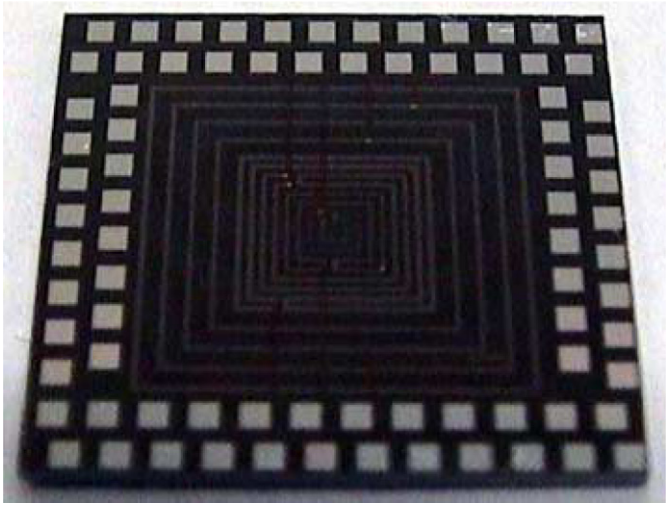

(a)

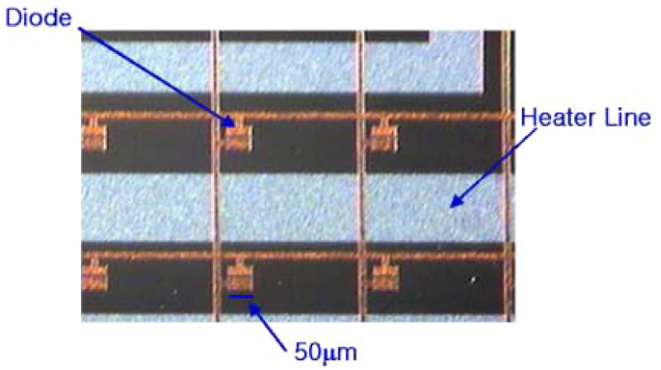

(b)

Fig. 4. Diode temperature sensor array. (a) Microfabricated diode temperature sensor array. (b) Diode temperature sensor.

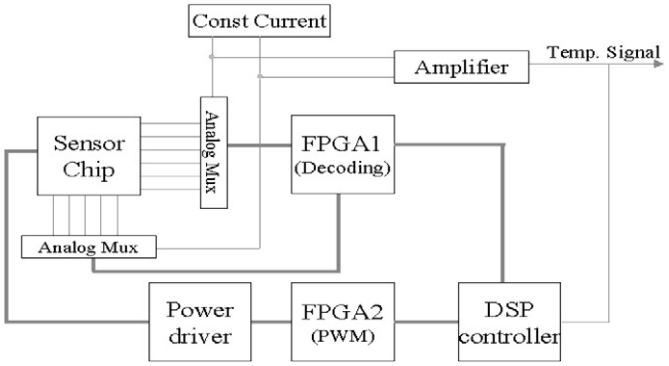

Fig. 5. Block diagram of the circuitry for the DTSA.

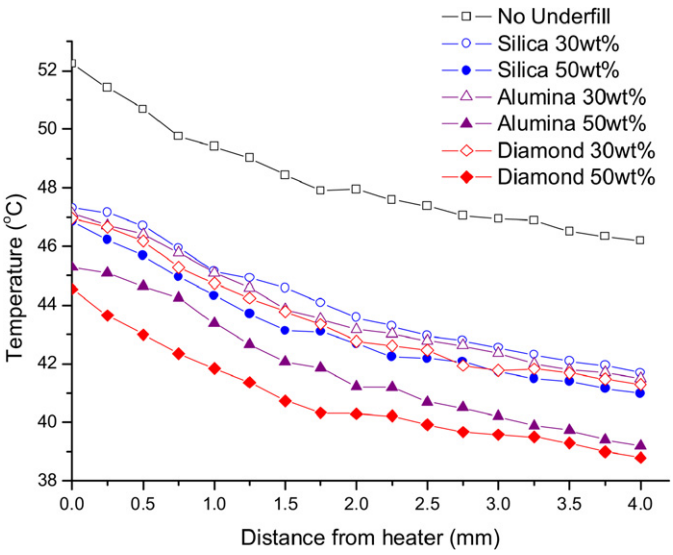

Fig. 6. Temperature distributions for flip chip packages.

through the power driver so that power dissipation from each heater is controlled [14].

The DTSA has been used for investigating the thermal characteristics of various underfill materials in a flip chip package [15]. The DTSAs are mounted on printed circuit boards with underfills which contain thermally conductive fillers such as silica (1.5 W/m K), alumina (36 W/m K), and diamond (2000 W/m K). Fig. 6 shows comparison of temperature profiles of the flip chip packages for various underfills. A large temperature reduction results from the addition of the underfill material, because it provides enhanced heat transfer path from the package to the board or the lead frame.

2.3. Microscale mass flow sensor

In many applications where chemical reactions, combustion, and semiconductor manufacturing processes are involved, a mass flow controller (MFC hereafter) is widely used for controlling the mass flow rate of a gas with an accuracy of 1% [16]. The MFC typically consists of a sensor tube, a bypass tube, and a control valve. The sensor tube in the MFC is the most critical part because the mass flow rate is sensed via a temperature difference caused by a heat transfer interaction between a heated tube wall and a gas stream flowing in the sensor tube. In a typical sensor tube, a single heater is centered on the outer surface of the sensor tube, and a pair of RTDs is symmetrically placed at the upstream and downstream of the heater. The mass flow rate is detected by measuring the temperature difference between the upstream sensor and the downstream sensor of the sensor tube. If the mass flow rate is sufficiently low, the temperature difference is proportional to the mass flow rate.

As the size of the systems used for biological reactions and processes, fuel cells, high performance heat exchangers and cooling devices, and chemical processes has been miniaturized, it has become necessary to develop an integrated mass flow sensor which can measure low mass flow rates accurately [17,18]. Hence, many investigators have been developing various microscale flow sensors using the manufacturing techniques developed for MEMS; these techniques include bulk-micromachining, surface micromachining, and LIGA-micromachining, to name a few [19,20]. The operating principle of the integrated microscale mass flow sensor that we have been developing is similar to that of the sensor tube in an MFC. In order to measure the mass flow rate through a microsystem, a temperature difference needs to be accurately measured. For this, the temperature sensors are fabricated on a quartz wafer

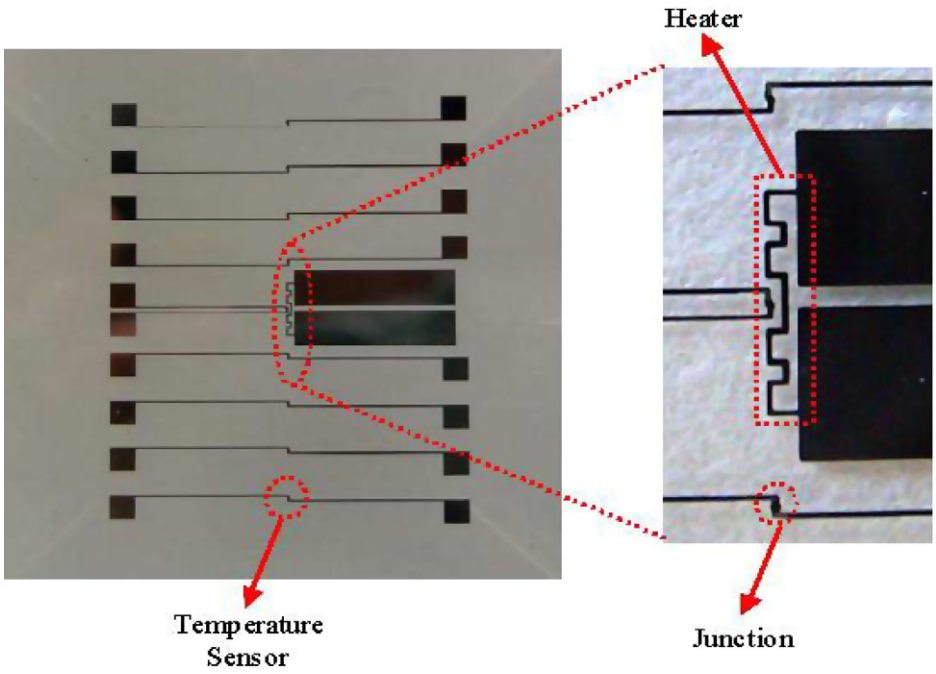

Fig. 7. Microscale mass flow sensor.

using the manufacturing processes that have been developed for the micro-thermal sensor array of Jang et al. [11], as shown in Fig. 7.

Even though only two sensors, an upstream sensor and a downstream sensor, are typically necessary, 9 temperature sensors are placed along the flow direction in order to study the thermal characteristics of an integrated mass flow sensor. A microchannel is made of PDMS (polydimethylsiloxane). The PDMS microchannel and the quartz wafer with an integrated mass flow sensor are bonded by plasma bonding, as shown in Fig. 8. An experimental investigation is underway for evaluating the characteristics of the microscale mass flow sensor.

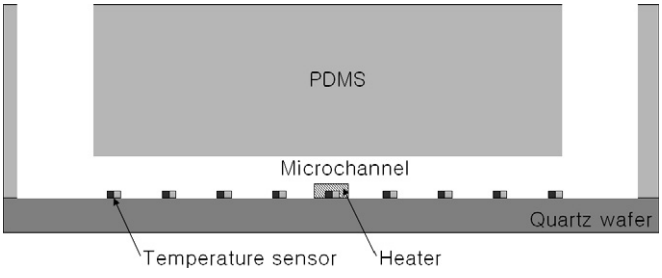

(a)

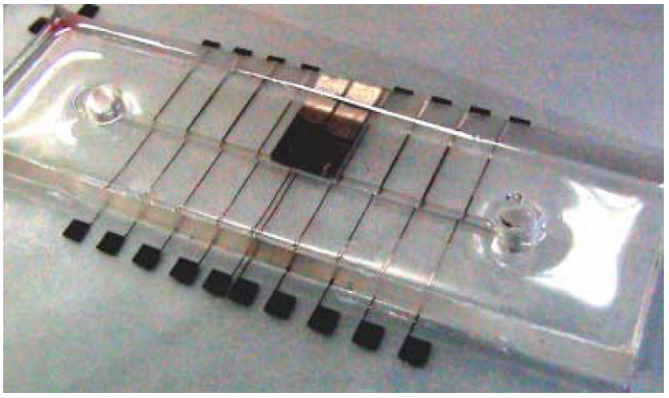

(b)

Fig. 8. PDMS microchannel with a microscale mass flow sensor. (a) Schematic diagram. (b) Photograph.

3. Modeling method

For most engineering purposes, detailed information such as velocity and temperature distributions is not required. We are usually concerned with estimating macroscopic aspects of a problem: average pressure drop across a channel or average heat transfer rate from a wall. If the prime interest of an investigator is the macroscopic quantities, it is wise to average the governing equations in the direction normal to the flow. This approach can lead to considerable simplification and be very useful, especially when the original problem requires significant time and money for complete solution. As a matter of fact, many types of averages are used in engineering. These include arithmetic mean, geometric mean, harmonic mean, logarithmic mean, and mean values of integration. Mean values of integration can be classified into time averaging, line averaging, area averaging, or volume averaging, depending on the independent variable for which integration is performed. Time averaging encountered in the study of turbulence and volume averaging used for flow through a porous medium are common examples of averaging methods encountered in chemical and mechanical engineering.

In this section, a modeling method developed for thermal design and optimization of microstructures will be presented. Many methods have been proposed and used by investigators working in the area of microscale heat transfer to analyze fluid

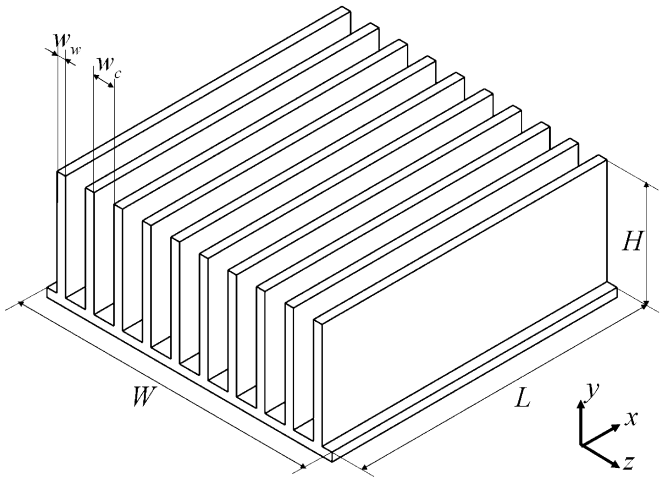

(a)

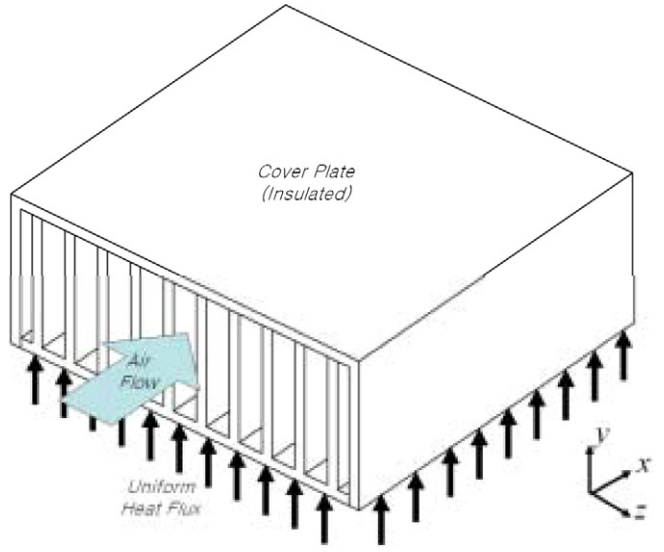

(b)

Fig. 9. Schematic of microchannel heat sink. (a) Dimensions of the heat sink. (b) Problem description.

flow and heat transfer in microstructures. The present paper is by no means a complete review of the modeling methods. Instead, an averaging method called the porous medium approach is introduced here. After the basic concept is introduced, the method will be applied to the thermal design of a microchannel heat sink developed for cooling microelectronic devices having high power density, in order to elucidate the method.

The problem under consideration in the present study concerns forced convection through a microchannel heat sink. A schematic of a microchannel heat sink is shown in Fig. 9. The direction of fluid flow is parallel to the x-axis. The top surface is insulated, and the bottom surface is uniformly heated. A coolant passes through a number of microchannels and takes heat away from a heat-dissipating electronic component attached below. In analyzing the problem, for simplicity, the flow is assumed to be laminar, incompressible, and both thermally and hydrodynamically fully-developed. All thermophysical properties are assumed to be constant. In addition, pumping power is assumed

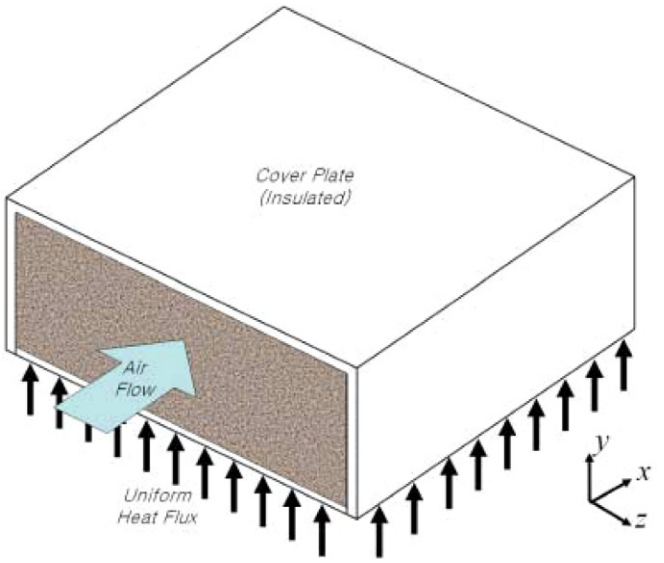

Fig. 10. Equivalent porous medium.

to be given. This condition means that the power required to drive the fluid through the microchannels is fixed.

In the averaging method, the microchannel heat sink is modeled as a fluid-saturated porous medium, as shown in Fig. 10. Mathematically, this is equivalent to averaging the velocity and temperature distributions in the direction perpendicular to the flow direction. This approach was applied to the microchannel heat sink by Tien and Kuo [23] and later extended by Kim and his coworkers [22,24,25]. Since the present system has a periodic structure in the spanwise direction, the representative elementary volume (REV hereafter) for averaging can be visualized as a slender cylinder aligned parallel to the z-axis. Then averaged quantities over the fluid and solid phases of the REV are defined, respectively, as follows:

$$\langle\phi\rangle^f = \frac{1}{w_c}\int_{w_c} \phi\, dz, \qquad \langle\phi\rangle^s = \frac{1}{w_w}\int_{w_w} \phi\, dz \tag{1}$$

The governing equations for the velocity and temperature fields in the microchannel heat sink are also established by averaging the momentum and energy equations. The governing equations and boundary conditions for fully-developed flow are given as follows [22,24]:

$$0 = -\frac{\partial\langle p\rangle^f}{\partial x} + \mu_f \frac{\partial^2\langle u\rangle^f}{\partial y^2} - \frac{\mu_f}{K}\varepsilon\langle u\rangle^f \tag{2}$$

$$\varepsilon\rho_f c_f \langle u\rangle^f \frac{\partial\langle T\rangle^f}{\partial x} = \frac{\partial}{\partial y}\left(k_{fe}\frac{\partial\langle T\rangle^f}{\partial y}\right) + h_i a\left(\langle T\rangle^s - \langle T\rangle^f\right) \tag{3}$$

$$\frac{\partial}{\partial y}\left(k_{se}\frac{\partial\langle T\rangle^s}{\partial y}\right) = h_i a\left(\langle T\rangle^s - \langle T\rangle^f\right) \tag{4}$$

$$\langle u\rangle^f = \langle v\rangle^f = 0, \quad \langle T\rangle^f = \langle T\rangle^s = T_w \quad \text{at } y = 0 \tag{5}$$

$$\langle u\rangle^f = \langle v\rangle^f = 0, \quad \frac{\partial\langle T\rangle^f}{\partial y} = \frac{\partial\langle T\rangle^s}{\partial y} = 0 \quad \text{at } y = H \tag{6}$$

where ε, K, a, k_{se}, and k_{fe} are porosity, permeability, wetted area per volume, effective conductivity of the solid and effective

conductivity of the fluid, respectively. Eq. (2) is the extended Darcy equation, which has been developed for describing fluid flow when the boundary effect cannot be neglected. Eqs. (3) and (4) are the so-called two-equation model, which treats the solid and the fluid as separate entities. For the microchannel heat sink,

$$\varepsilon = \frac{w_c}{w_c + w_w}, \qquad a = \frac{2}{w_c + w_w}$$
$$k_{se} = (1-\varepsilon)k_s, \qquad k_{fe} = \varepsilon k_f \tag{7}$$

To solve the governing equations, Eqs. (2)–(4), K and h_i should be determined in advance. The permeability K is related to the viscous shear stress caused by the fins, and the interstitial heat transfer coefficient h_i is related to the convective heat transfer from the fins. These parameters have been typically obtained from either experimental investigations or numerical simulations. For the present configuration, however, these parameters can be determined analytically using an approximation. Kim and his co-workers assume that the characteristics of pressure drop across and heat transfer from the fins are similar to those found for the Poiseuille flow between two infinite parallel plates that are subject to a constant heat flux in the streamwise direction [22]. They have obtained

$$K = \frac{\varepsilon \langle u \rangle^f}{-\mu\, dp/dx} = \frac{\varepsilon w_c^2}{12} \tag{8}$$

$$h_i = \frac{q''}{T_w - \langle T \rangle^f} = \frac{Nu_{i,\infty} k_f}{2w_c} \tag{9}$$

where the value of $Nu_{i,\infty}$ is 10. These approximate values for K and h_i are shown to be valid when the aspect ratio is of the order of one or larger.

Once the permeability and the interstitial heat transfer coefficient are determined, analytical solutions for velocity and temperature distributions can be obtained by solving the governing equations, Eqs. (2)–(4), with boundary conditions, Eqs. (5)–(6). The analytical solutions for dimensionless velocity and temperature distributions are as follows:

$$U = A\cosh\left(\sqrt{\frac{\varepsilon}{Da}}Y\right) + B\sinh\left(\sqrt{\frac{\varepsilon}{Da}}Y\right) - P \tag{10}$$

$$\theta_f = \frac{P}{1+C}\left[-\frac{1}{2}Y^2 + C_1 Y + C_6 - C_3\cosh\left(\sqrt{\frac{D(1+C)}{C}}Y\right) - C_4\sinh\left(\sqrt{\frac{D(1+C)}{C}}Y\right) + C_7\left\{\cosh\left(\sqrt{\frac{\varepsilon}{Da}}Y\right) + \frac{1-\cosh(\sqrt{\frac{\varepsilon}{Da}})}{\sinh(\sqrt{\frac{\varepsilon}{Da}})}\sinh\left(\sqrt{\frac{\varepsilon}{Da}}Y\right)\right\}\right] \tag{11}$$

$$\theta_s = P\left[\frac{Da}{\varepsilon}\left\{\cosh\left(\sqrt{\frac{\varepsilon}{Da}}Y\right) + \frac{1-\cosh(\sqrt{\frac{\varepsilon}{Da}})}{\sinh(\sqrt{\frac{\varepsilon}{Da}})}\sinh\left(\sqrt{\frac{\varepsilon}{Da}}Y\right) - 1\right\} - \frac{1}{2}Y^2 + C_1 Y\right] - C\theta_f \tag{12}$$

where

$$Y = \frac{y}{H}, \qquad U = \frac{\langle u \rangle^f}{u_m}, \qquad Da = \frac{K}{H^2}$$
$$\theta_s = \frac{\langle T \rangle^s - T_w}{\frac{q_w H}{(1-\varepsilon)k_s}}, \qquad \theta_f = \frac{\langle T \rangle^f - T_w}{\frac{q_w H}{(1-\varepsilon)k_s}} \tag{13}$$

Mathematical expressions for the coefficients appearing in the above solutions can be found in [22].

Fig. 11 shows a comparison of the velocity and temperature distributions calculated by the averaging method and numerical simulation. The results obtained from numerical simulation can be regarded as exact. Hence they are used as a basis for comparison. As shown in this figure, the results obtained from the averaging method are in close agreement with the exact values. Because the analytical solutions obtained from the porous-medium approach are much simpler and easier to handle than numerical results, they are helpful for identifying and studying the effects of variables of engineering importance. So the extension to more practical research, such as optimization of the microchannel heat sink, is possible without tedious numerical computations. The example of microchannel heat sink optimization follows next.

The concept of thermal resistance is used to evaluate the thermal performance of microchannel heat sinks. The total thermal resistance is defined as the temperature difference between two points of concern per unit heat flow rate, i.e.,

$$R_{\theta,\mathrm{tot}} = \frac{T_{s,\mathrm{out}} - T_{b,\mathrm{in}}}{q} \tag{14}$$

Thus, the thermal resistance for a constant-heat-flux condition is directly proportional to the temperature difference between the heat sink base temperature at the exit and the coolant temperature at the inlet. Eq. (14) can be decomposed into two terms as follows:

$$R_{\theta,\mathrm{tot}} = \frac{T_{s,\mathrm{out}} - T_{b,\mathrm{out}}}{q} + \frac{T_{b,\mathrm{out}} - T_{b,\mathrm{in}}}{q} \tag{15}$$

Using the energy balance, we can obtain

$$R_{\theta,\mathrm{tot}} = \frac{T_{s,\mathrm{out}} - T_{b,\mathrm{out}}}{q} + \frac{1}{\dot{m}c_f} \tag{16}$$

where the first term on the right-hand side is known as the convective resistance, $R_{\theta,\mathrm{conv}}$, and the second term the capacity resistance, $R_{\theta,\mathrm{cap}}$. The former is related to heat transfer from the fins to the coolant, and the latter is responsible for the temperature rise of the coolant from the inlet to the exit.

The final goal is to determine the important dimensions for which the total thermal resistance is minimized when a pumping power is specified. From the definition of bulk-mean temperature, the convective thermal resistance of the microchannel heat sink can be represented by

$$R_{\theta,\mathrm{conv}} = \frac{\theta_{f,b} H}{(1-\varepsilon)k_s LW} + \left(\frac{1}{Nu_\infty} - \frac{1}{Nu_{i,\infty}}\right)\frac{w_c(w_c + w_w)}{k_f LWH} \tag{17}$$

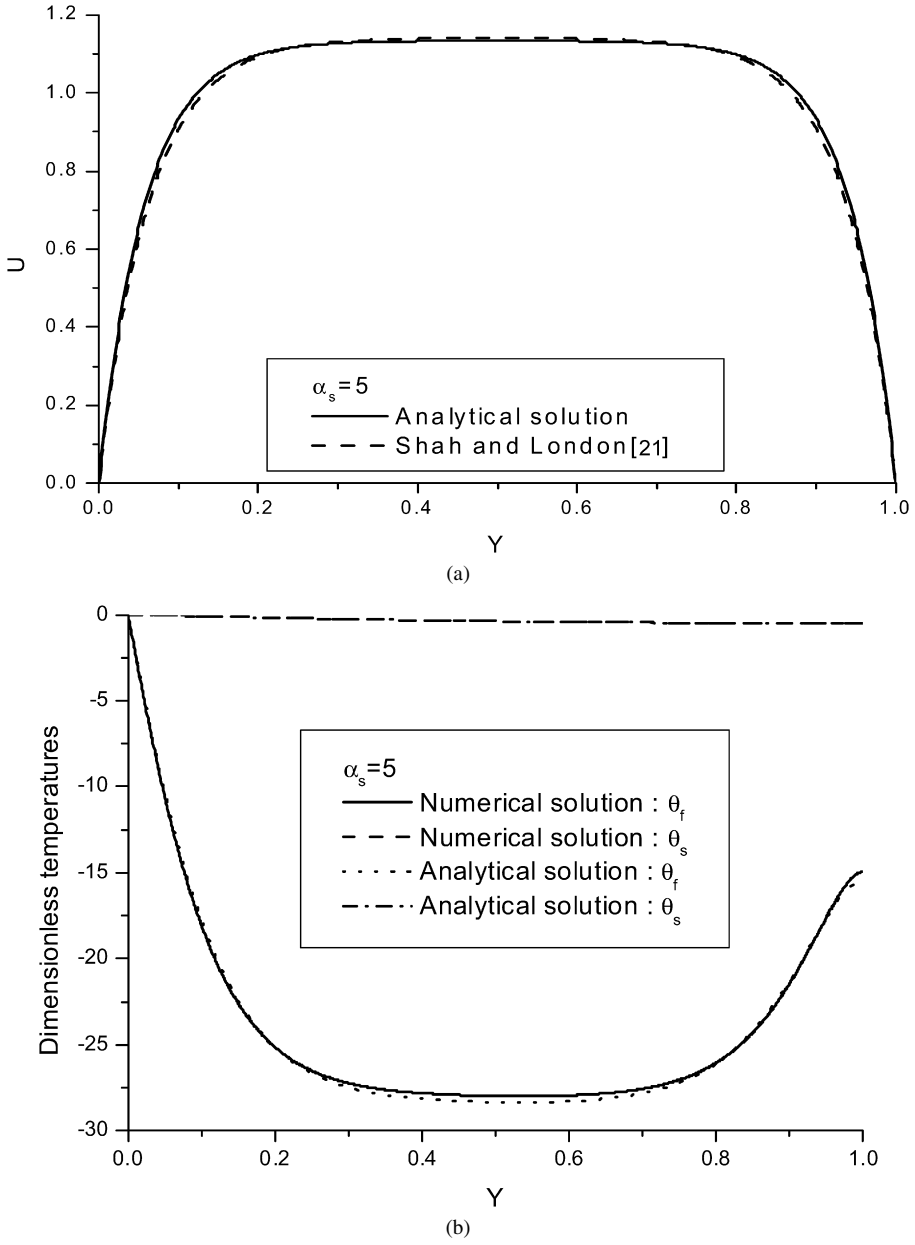

Fig. 11. Validation of the averaging method: (a) velocity distribution, and (b) temperature distributions.

where the bulk-mean temperature adopted in the porous-medium approach is

$$\theta_{f,b} = \int_0^1 U\theta_f \, dY \tag{18}$$

The second term on the right-hand side of Eq. (17) is included to account for the difference between the conventional bulk-mean temperature and the bulk-mean temperature defined in Eq. (18). The value for Nu_∞ is 8.235, which is the Nusselt number based on the bulk-mean temperature for heat transfer between two infinite parallel plates subject to a constant heat flux. For a large-aspect-ratio microchannel, Eq. (17) reduces to

$$R_{\text{conv}} = \frac{1}{3}\frac{(w_c + w_w)H}{k_s w_w W L} + \frac{w_c(w_c + w_w)}{Nu_\infty k_f H W L} \tag{19}$$

The design variables for thermal optimization of a microchannel heat sink are the fin thickness and the channel width; for optimal values of these variables, the total thermal resistance is minimized. Equating the first derivatives of Eq. (19) with respect to w_w and w_c to zero yields respectively the optimal fin thickness and channel width for the microchannel heat sink as

$$w_w = \frac{H\sqrt{k_f Nu_\infty}}{\sqrt{6k_s}} \tag{20}$$

$$w_c^6 + \frac{H\sqrt{k_f Nu_\infty}}{\sqrt{6k_s}} w_c^5 = \frac{3Nu_\infty^2 k_f^2 \mu_f W L^3 H}{\rho^2 C_p^2 P_p} \tag{21}$$

where P_p is the fixed pumping power.

Fig. 12(a) shows the optimized design variables and the corresponding thermal resistances obtained both from the averag-

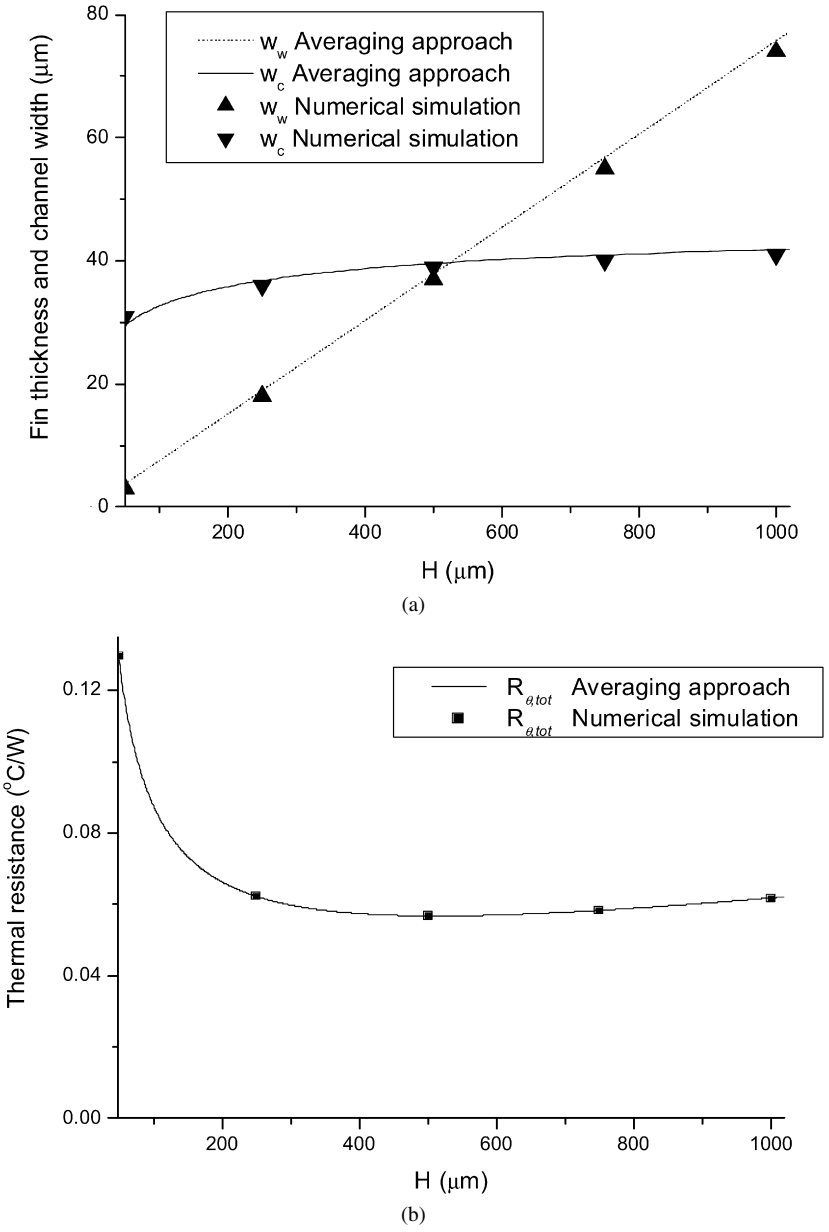

Fig. 12. Optimized results: (a) w_w and w_c, and (b) R_{tot}.

ing method and from numerical simulation for various aspect ratios. The results for the design variables obtained analytically from the averaging method are in close agreement with those obtained numerically. The thermal resistances obtained from the averaging method are shown to match well with the numerical results regardless of the aspect ratio, as shown in Fig. 12(b). The averaging method described above can be easily extended to the problems for developing flows [26] and to the problems subject to the uniform wall temperature condition [27] as well.

As demonstrated in this case study, the averaging method is very accurate but simpler than numerical simulation. Therefore, the averaging method is recommended for the thermal design and optimization of microstructures. As long as the characteristic length scale in the averaging direction is smaller than that in the other direction, the averaging method provides reasonable results. Whether the averaging method is still applicable to a nano-scale structure depends on the type of fluid and the channel size and geometry. As long as the Knudsen number is on the order of 0.1 or smaller, the present approach can be safely used. The extension to a problem with a larger Knudsen number is under investigation.

4. Conclusion

In the present study, various sensors developed for experimental investigations and a modeling method for analyzing the thermal characteristics of a microstructure encountered in micro-mechanical engineering are described. In the first part, sensors that can be used to measure the temperature distributions at the surface of a microstructure and the mass flow rate passing through it are introduced. These include the micro-

thermal sensor array, the diode temperature sensor array, and the microscale mass flow sensor. The characteristics and manufacturing processes for the sensors are explained. In the second part, a modeling method based on averaging is explained. The thermal optimization of a microchannel heat sink is conducted to elucidate the method in the context of thermal design of a microstructure.

Acknowledgements

This work was supported by the Korea Science and Engineering Foundation (KOSEF) through the National Research Lab. Program funded by the Ministry of Science and Technology (No. M10600000224O6J000022410).

References

[1] C. Tien, A. Majumdar, F.M. Gerner, Microscale Energy Transport, Taylor & Francis Press, USA, 1998.
[2] D.L. Blackburn, Thermal measurement of semiconductor devices, in: Thermal Challenges in Next Generation Electronic Systems, Int. Conference THERMS 2002, Santa Fe, NM, 2002, pp. 13–16.
[3] S.B. Choi, R.F. Barron, R.O. Warrington, Fluid flow and heat transfer in microtubes, ASME Micromech. Sens. Actuators Syst. 32 (1991) 123–134.
[4] M.M. Rahman, Measurements of heat transfer in microchannel heat sinks, Int. Commun. Heat Mass Transfer 27 (2000) 495–506.
[5] T.M. Harms, M.J. Kazmierczak, F.M. Gerner, Developing convective heat transfer in deep rectangular microchannels, Int. J. Heat Fluid Flow 20 (1999) 149–157.
[6] H.-C. T. Yeh, Fabrication and cooling test of high aspect-ratio electroplated microchannels, M.S. Thesis, Dept. of Mechanical Engineering, UCLA, USA, 1998.
[7] Q. Lin, S. Wu, Y. Yien, Y.-C. Tai, C.-M. Ho, MEMS impinging jet cooling, J. MEMS 2 (2000) 137–142.
[8] Y.M. Shwarts, V.L. Borblik, N.R. Kulis, E.F. Venger, V.N. Sokolov, Limiting characteristics of diode temperature sensors, Sens. Actuators A 86 (2000) 197–205.
[9] J. Kim, M. Whitten, R.W. Quine, T.S. Kalkur, Design and development of a diode array for use in boiling heat transfer, J. Japan Soc. Microgravity Appl. 15 (1998) 202–207.
[10] R.S. Figliola, D.E. Beasley, Theory and Design for Mechanical Measurement, second ed., John Wiley & Sons, Inc., New York, 1998 (Chapter 8).
[11] S.P. Jang, S.J. Kim, K.W. Paik, Experimental investigation of thermal characteristics for a microchannel heat sink subject to an impinging jet using a micro-thermal sensor array, Sens. Actuators A 105 (2003) 211–214.
[12] L. Shi, O. Kwon, A. Miner, A. Majumdar, Design and batch-fabrication of probes for sub-100 nm scanning thermal microscopy, J. MEMS 3 (2001) 370–378.
[13] A.S. Sedra, K.C. Smith, Microelectronic Circuits, fourth ed., Oxford Univ. Press, New York, 1998.
[14] W. Bolton, Mechatronics: Electronic Control Systems in Mechanical and Electrical Engineering, Longman, USA, 2000.
[15] W.S. Lee, I.Y. Han, J. Yu, S.J. Kim, T.Y. Lee, Thermal characterization of thermally conductive underfill for a flip-chip package using novel temperature sensing technique, in: 6th Electronics Packaging Technology Conference (EPTC) 2004, Singapore, 2004, A2.4.
[16] S.J. Kim, S.P. Jang, Experimental and numerical analysis of heat transfer phenomena in a sensor tube of a mass flow controller, Int. J. Heat Mass Transfer 44 (2001) 1711–1724.
[17] M. Richter, P. Woias, D. Weiß, Microchannels for applications in liquid dosing and flow-rate measurement, Sens. Actuators A 62 (1997) 480–483.
[18] A. Rasmussen, M.E. Zaghloul, In the flow with MEMS, IEEE Circuits and Devices Magazine 14 (1998) 12–25.
[19] N.T. Nguyen, Micromachined flow sensors—a review, Flow Meas. Instrum. 8 (1997) 7–16.
[20] H. Ernst, A. Jachimowicz, G.A. Urban, High resolution flow characterization in Bio-MEMS, Sens. Actuators A 100 (2002) 54–62.
[21] R.K. Shah, A.L. London, Laminar Flow Forced Convection in Ducts, Academic Press, London, 1978.
[22] S.J. Kim, D. Kim, Forced convection in microstructures for electronic equipment cooling, ASME J. Heat Transfer 121 (1999) 639–645.
[23] C.L. Tien, S.M. Kuo, Analysis of forced convection in microstructures for electronic system cooling, in: Proc. Int. Symp. Cooling Technology for Electronic Equipment, Honolulu, HI, 1987, pp. 217–226.
[24] S.J. Kim, D. Kim, D.Y. Lee, On the local thermal equilibrium in microchannel heat sinks, Int. J. Heat Mass Transfer 43 (2000) 1735–1748.
[25] S.J. Kim, J.W. Yoo, S.P. Jang, Thermal optimization of a circular-sectored finned tube using a porous medium approach, ASME J. Heat Transfer 124 (2002) 1026–1033.
[26] D. Kim, S.J. Kim, Compact modeling of fluid flow and heat transfer in straight fin heat sinks, ASME J. Electronic Packaging 126 (2004) 247–255.
[27] D.K. Kim, S.J. Kim, Averaging approach for microchannel heat sinks subject to the uniform wall temperature condition, Int. J. Heat Mass Transfer 49 (2006) 695–706.